Paper:

Retinal Blood Vessel Segmentation Using Extreme Learning Machine

Fan Guo, Da Xiang, Beiji Zou†, Chengzhang Zhu, and Shengnan Wang

School of Information Science and Engineering, Central South University
Changsha, Hunan 410083, China
†Corresponding author, E-mail: bjzou@csu.edu.cn
[Received March 19, 2017; accepted September 4, 2017]

Extreme learning machine (ELM) is an effective machine learning technique that widely used in image processing. In this paper, a new supervised method for segmenting blood vessels in retinal images is proposed based on the ELM classifier. The proposed algorithm first constructs a 7-D feature vector using multi-scale Gabor filter, Hessian matrix and bottom-hat transformation. Then, an ELM classifier is trained on gold standard examples of vessel segmentation images to classify previous unseen images. The algorithm was tested on the publicly available DRIVE database – a digital image database for vessel extraction. Experimental results on both real-captured images and public database images demonstrate that our method shows comparative performance against other methods, which make the proposed algorithm a suitable tool for automated retinal image analysis.

Keywords: retinal image, vessel segmentation, Extreme Learning Machine (ELM), Gabor filter, Hessian matrix, bottom-hat transformation

1. Introduction

The study of the retinal vasculature is very important for three reasons: Firstly, it is the only part of the blood circulation system that can be observed directly; Secondly, a number of systemic conditions can be diagnosed by the detection of lesions in the retinal vasculature [1]; Thirdly, The manual labeling of retinal blood vessels is very time-consuming, which requires training and skill. Therefore, an automated reliable method of vessel segmentation would be valuable for the early detection of changes in the retinal vasculature. Besides, just like the detection of artery region for magnetic resonance (MR) image [2], retinal blood vessel segmentation is also very useful for many automated computer aided systems to screen and diagnose some diseases.

This paper presents a new supervised method for segmenting blood vessels by using an ELM classifier. The feature vector adopted in the proposed method is based on multi-scale Gabor filter response, Hessian matrix measure, and the bottom-hat transformation. The classifier based on the ELM provides good generalization performance at very fast learning speed since its parameters can be analytically determined rather than being tuned. Using the ELM classifier, all the image pixels are divided into two pixel classes: the vessel pixels and non-vessel pixels. We test the proposed algorithm on the public digital retinal images for vessel extraction (DRIVE) database. The image database consists of 40 manually labeled images with gold standard. The obtained performance metrics illustrate that the proposed method outperforms most of the state of the art retinal vessel segmentation methods in term of segmentation performance. Moreover, the method is computationally fast in training and classification procedures.

The paper is organized as follows. In Section 2, the related works about retinal vessel segmentation are reviewed. Section 3 describes the proposed algorithm in details. Experimental results of the proposed algorithm on the public image database are discussed in Section 4. In Section 5, we discuss some critical issues related to the proposed method, and the paper is concluded in Section 6.

2. Related Work

Many researchers have proposed their methods for segmenting blood vessels in retinal images. References [3, 4] give a detailed review of these methods. Generally, the vessel segmentation algorithms can be divided into the unsupervised and supervised methods.

2.1. Unsupervised Methods

There are many unsupervised methods that can be used for retinal blood vessel segmentation. These methods include matched filtering, morphological processing, vessel tracking, multi-scale analysis, and model-based algorithms. The matched filtering method adopts the piecewise linear approximation, the decrease in vessel diameter along vascular length, and the Gaussian-like intensity profile of retinal blood vessels and uses a kernel based on a Gaussian or its derivatives to enhance the vessel features in the retinal image [5, 6]. For example, Oliveira et al. [7] develops an unsupervised segmentation procedure for the segmentation of retinal vessels images using a combined matched filter, Frangi filter and Gabor Wavelet Filter. Singh et al. [8] propose a matched filter approach

with the Gumbel probability distribution function as its kernel to improve the performance of retinal blood vessel segmentation. Other methods like mathematical morphology combined with curvature evaluation [9] and centreline detection [10, 11] are also used to segment retinal vessel. Vessel tracking method [12] is also used for segmenting a vessel between two points using local information. The method aims at a single vessel rather than the entire vasculature. Recently, the multi-scale approaches which based on scale-space analysis have drawn the attention of many researchers. For example, Frangi et al. exam the multi-scale second-order local structure of an image (Hessian) and obtain a vesselness measure on the basis of eigenvalue analysis of the Hessian [13]. Dai et al. [14] propose a multi-scale line filter which is integrated with phase congruency to detect the network of vessels in retinal images. The line filter can reduce the influence of step edges compared with Gaussian matched filter. Masooomi et al. [15] use multi-scale line detection and nonsubsampled contourlet transform to automatically extract blood vessels from color retinal images. The model-based approaches include the vessel profile models [16–19], active contour models [20], graph-cut models [21] and geometric models based on level sets [22].

2.2. Supervised Methods

The supervised segmentation methods use ground truth data to classify vessels based on certain given features. For example, Niemeijer et al. [23] extracted a feature vector for each pixel that consists of the Gaussian and its derivatives at multiple scales, and then estimated the probability of the pixel belonging to a vessel by using a K-nearest neighbor algorithm. Staal et al. [24] presented a vessel segmentation system based on extraction of image ridges, which coincide approximately with vessel centerlines. The ridges are used to compose primitives in the form of line elements. In [25], each image pixel is classifies as vessel or non-vessel based on the pixel's feature vector. These feature vectors are composed of the pixel's intensity and two-dimensional Gabor wavelet transform responses taken at multiple scales. Ricci and Perfetti [26] proposed a retinal vessel segmentation method based on line operators. Two orthogonal line detectors along with the grey level of the target pixel are employed to construct a feature vector for supervised classification using a support vector machine (SVM). Lupascu et al. [1] constructed a 41-D feature vector to encode information on the local intensity structure, spatial properties, and geometry at multiple scales. An AdaBoost classifier is used in the method for classifying previously unseen images. In [27], a 7-D vector composed of gray-level and moment invariants-based features is computed for pixel representation. You et al. [28] used the complex wavelet followed by calculating the line strength [26] to compute the feature vector, and the SVM is employed for pixel classification. Nowadays, the artificial neural network (ANN)-based method has achieved both scientific and economic success. For example, Nandy et al. [29] propose an automated segmentation scheme of retinal vasculature using Gabor filter and artificial neural network. Ceylan et al. [30] propose a method for automatic blood vessel extraction from retinal image using complex wavelet transform and complex-valued artificial neural network. Ding et al. [31] adopt a neural network based supervised segmentation algorithm for retinal vessel delineation. Melinscak et al. [32] use a GPU implementation of deep max-pooling convolutional neural networks to segment blood vessels. Li et al. [33] present a cross-modality learning method for vessel segmentation in retinal images. The method uses a wide and deep neural network with strong induction ability to model the transformation. However, although good segmentation accuracy can be obtained in a classifier trained by an ANN, a relatively long time is needed in the training phase for the ANN-based method. In this study, we have proposed an ELM based classifier which is computationally simple and faster than the ANN-based methods.

3. Proposed Algorithm

3.1. Algorithm Framework

The basic idea of our algorithm is to segment retinal blood vessel from the extracted feature vectors in a supervised way. To divide retinal image pixels into vessel and non-vessel pixels, an ELM classifier is adopted for this purpose.

Figure 1 depicts the algorithm framework of our vessel segmentation system. As can be seen in the figure, the proposed algorithm is divided into four major steps. The first step is to obtain enhanced retinal images for both training and testing databases by using the guided filter [34] in the preprocessing phase.

The second step is to extract a 7-D feature vector of the enhanced retinal images in both training and testing databases. These feature vectors include multi-scale Gabor filter, Hessian matrix measure and bottom-hat transformation, which encode information on geometry at multiple scales, local intensity structure and image morphological property.

In the third step, an ELM classifier is trained on the gold standard examples of vessel and non-vessel pixels, and then used for classifying previously unseen images in testing database by using the parameters obtained from the training phase.

In the last step, some unwanted ledges and disconnected small vessel parts are removed in the post-processing phase. A comparative study and a quantitative evaluation are proposed with other methods, which demonstrate that comparable or even better quality results can be obtained by the proposed method.

3.2. Image Preprocessing

In the preprocessing phase, the guided filter algorithm [34] is used here to enhance the input retinal images for both training and testing databases. Specifically,

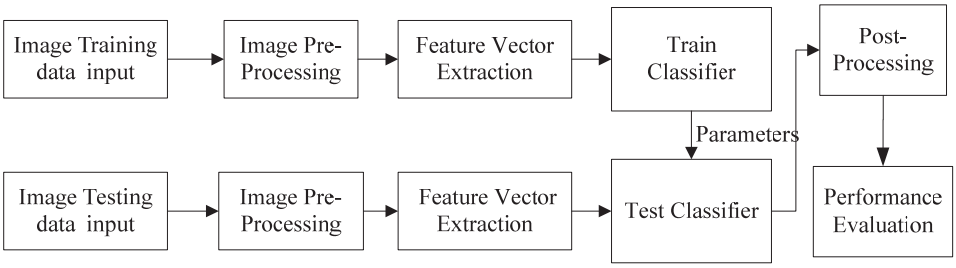

Fig. 1. Our vessel segmentation framework.

for the input image, it is assumed that enhanced retinal image is a linear transform of the input (guidance) image $I(\boldsymbol{x})$ in a window ω_k centered at pixel $\boldsymbol{x} = (x, y)$.

$$\hat{I}(\boldsymbol{x}) = \bar{a}_k I(\boldsymbol{y}) + \bar{b}_k, \quad \forall \boldsymbol{y} \in \omega_k \quad \ldots\ldots\ldots \quad (1)$$

where a_k and b_k are linear coefficients assumed to be constant in ω_k. To make the difference between the output $\hat{I}(\boldsymbol{x})$ and the input $I(\boldsymbol{x})$ as small as possible, the two parameters a_k and b_k can be defined as:

$$a_k = \frac{\frac{1}{|\omega|}\sum_{x\in\omega_k} I(x)^2 - u_k \bar{I}_k}{\sigma_k^2 + \varepsilon} \quad \ldots\ldots\ldots \quad (2)$$

$$b_k = \bar{I}_k - a_k u_k \quad \ldots\ldots\ldots\ldots\ldots\ldots \quad (3)$$

In Eq. (2), the small variable ε is a regulation parameter to prevent ω_k from being too large. In our experiment, we set ε to be 0.01–0.03. $|\omega|$ is the number of pixels in the filtering window. u_k and σ_k are the mean and variance vector of the pixels in kth filtering window, respectively. $\bar{I}$ is the pixel mean value of the input image I in ω_k, which can be calculated as:

$$\bar{I}_k = \frac{1}{|\omega|}\sum_{i\in\omega_k} I_i \quad \ldots\ldots\ldots\ldots\ldots\ldots \quad (4)$$

Similarly, we can obtain the pixel mean value of the a_k and b_k in ω_k as $\bar{a}_k$ and $\bar{b}_k$. By substituting $\bar{a}_k$ and $\bar{b}_k$ into (1), we get the enhanced retinal image $\hat{I}(\boldsymbol{x})$. Some enhancement results are shown in **Fig. 2**. From the figure, one can clearly see that the blood vessels in the retinal images are more obvious than those in the original input images, which makes it much easier for identifying vessel feature and structure in the following steps.

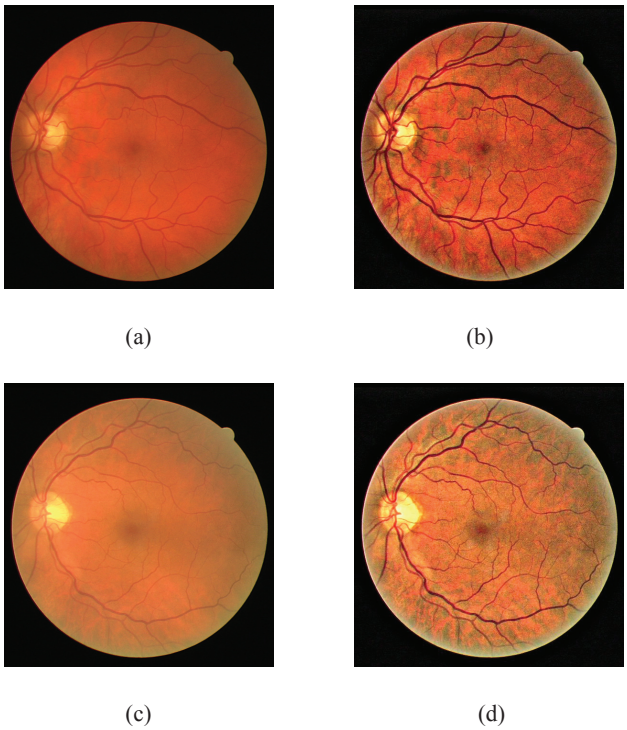

Fig. 2. Image preprocessing results. (a) and (c) are original input retinal image. (b) and (d) are the enhanced results obtained by using guided filter.

3.3. Feature Vector

The feature vector can be regarded as the quantifiable measurement for each pixel. Better feature vector can make the classifier successfully differentiate the blood vessels and the bright and dark lesions. For the proposed algorithm, a 7-D vector is used for representing the retinal image features. The 7 features include the intensity of each pixel in the green channel (one feature), a Gabor filter response at multiple scales (four features) for eliminating the dark lesions, the norm of the Hessian matrix (one feature) for distinguishing between background and vessel pixels, and the bottom-hat transformation (one feature) for eradicating bright lesions. Since the green channel has a higher contrast between the vessels and the background than other channels, thus all the features are extracted from the green channel of the enhanced RGB colored retinal image obtained using the guided filter as a preprocessing.

3.3.1. Multi-Scale Gabor Filter

A Gabor filter is a linear filter which has been broadly used for multi-scale and multidirectional edge detection. The Gabor filter can be fine-tuned to particular frequencies, scales, and directions, and therefore acts as a low-level feature extractor and background noise suppressor. The impulse response of a Gabor filter kernel is defined by the product of a Gaussian kernel and a complex sinusoid. Thus the filter can be written as [25, 35]:

$$g(x,y) = \exp\left\{-0.5\left(\frac{x'^2 + \gamma y'^2}{2\sigma^2}\right)\right\}\exp\left\{i\left(2\pi\frac{x'}{\lambda} + \varphi\right)\right\} \quad \ldots\ldots\ldots\ldots\ldots\ldots \quad (5)$$

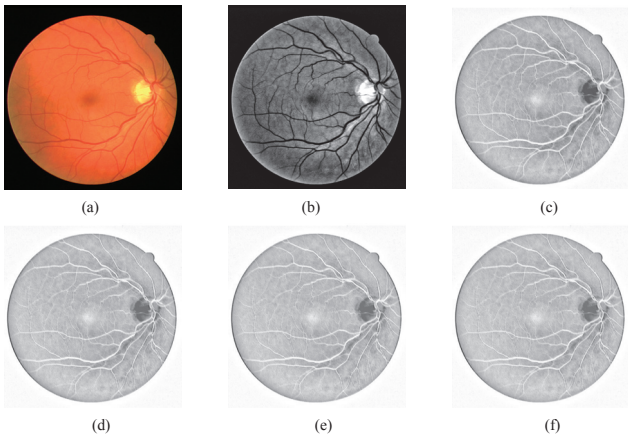

Fig. 3. Multi-scale Gabor feature. (a) Input retinal image. (b) Green channel of the enhanced retinal image. (c)–(f) Gabor filter response at scale 2, 4, 6, 8 respectively. The images in (c)–(f) are inverted for better visibility.

where σ is the scale of the Gaussian envelope, φ is the phase offset, λ is the wavelength of the sinusoidal factor, γ is the spatial aspect ratio. Let θ be the orientation, then $x' = x\cos\theta + y\sin\theta$, and $y' = -x\sin\theta + y\cos\theta$.

We applied the Gabor filter to the green channel of the colored retinal image. As can be seen in Eq. (5) the filter is obtained by a 2-D convolution operator. In our experiment, the maximum filter response over the angle θ, spanning $[0, 11\pi/12]$ in steps of $\pi/12$, is computed for each pixel in the image at different scales ($\sigma = \{2,4,6,8\}$). The maximum response across the orientation at a scale is taken as the pixel feature vector. The feature space is normalized to zero mean and unit standard deviation by applying the normal transformation. **Fig. 3** shows the results of multi-scale Gabor filter response at scale 2, 4, 6, 8 respectively. The reason why we choose such scales is that we want to combine both local feature (relatively high frequency) and global feature (relatively low frequency) by changing the scale value from 2 to 8. In our experiment, we also find that if other scales are selected, some observations can be obtained: i) the running time of Gabor filter response increases as the scale value become larger. For example, the running time of Gabor filter at scale $\{2,4,6,8\}$ is about 4s for the input image shown in **Fig. 3(a)**, while the time at scale $\{20,40,60,80\}$ is about 6 s; and ii) there is little difference of Gabor response image when we convert the scale $\{2,4,6,8\}$ to $\{1,3,6,9\}$ or $\{2,3,4,5\}$ for **Fig. 3**, which demonstrates that the influence of the scale value is very limited in the multi-scale Gabor filter when the orientation of the filter is fixed. The experiments on other test retinal images also confirm the observations.

Besides, one can clearly see that the multi-scale Gabor filter is adopted to extract the edge of the blood vessel in different scales. The main advantage of the multi-scale method is that the minute details can be detected in small scale, but the detected results may be easily disturbed by the noise. While the large scale has a better immunity to the noise, but some minute details will be lost in the scale.

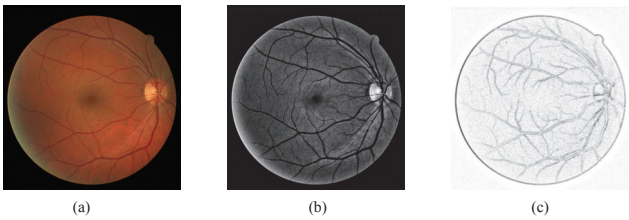

Fig. 4. Hessian matrix measure. (a) Input retinal image. (b) Green channel of the enhanced retinal image. (c) Fobenius norm of the Hessian. The images in (c) are inverted for better visibility.

By fusing the image information in different scales, the detection performance of vessel edge can be greatly improved. Since the blood vessels are enhanced by using the guided filter in the preprocessing stage, the edge feature of the blood vessels can be better depicted by using the multi-scale Gabor filter.

3.3.2. Hessian Matrix Measure

For typical fundus camera images, blood vessels are darker than the background. Therefore, Hessian matrix measure [1, 36] can be used to handle this kind of images. The numerical estimate of the Hessian of the intensity image in the scale space at each point $L(x,y)$ contains partial derivatives computed by convolving the intensity function with the first derivatives of a Gaussian kernel, which identifies the spatial scale of the result and reduces the effects of noise and discretization.

$$H(x,y) = \begin{bmatrix} \dfrac{\partial^2 L}{\partial x^2} & \dfrac{\partial^2 L}{\partial x \partial y} \\ \dfrac{\partial^2 L}{\partial y \partial x} & \dfrac{\partial^2 L}{\partial y^2} \end{bmatrix} = \begin{bmatrix} L_{xx} & L_{xy} \\ L_{yx} & L_{yy} \end{bmatrix} \quad . \quad . \quad (6)$$

Thus, the Fobenius norm of the Hessian can be written as:

$$\|H\| = \sqrt{L_{xx}^2 + 2L_{xy}^2 + L_{yy}^2} \quad . \quad . \quad . \quad . \quad . \quad . \quad . \quad . \quad (7)$$

There are many reasons for using the norm of the Hessian to distinguish between background and vessel pixels. On the one hand, since the magnitude of the derivatives of the intensities is small, thus the above Frobenius norm is low in the background where no structure and contrast is present and the eigenvalues are small. On the other hand, in regions with high contrast compared to the background, the norm will become larger since at least one of the eigenvalues will be large. The Fobenius norm image containing the enhanced blood vessels are shown in **Fig. 4**.

3.3.3. Bottom-Hat Transformation

Bottom-hat transformation is a kind of morphological transformation. If the intensity values in a gray-level image are thought of as elevations, then a scene is composed of mountain tops (brightest points) and valley lows

Fig. 5. Bottom-hat transformation. (a) Input retinal image. (b) Green channel of the enhanced retinal image. (c) Bottom-hat transformation result. The images in (c) are inverted for better visibility.

(darkest regions). Uneven contrast in an image will often degrade threshold isolation of adjacent mountain tops between valleys. Since the intensity of blood vessel is generally lower than that of background, thus the bottom-hat transformation is used to extract feature vector. This transformation can be written as [37]:

$$I_{th}^{\theta} = (I \bullet S_e^{\theta}) - I \quad \ldots\ldots\ldots\ldots\ldots\ldots (8)$$

$$Is_{th} = \sum_{\theta \in A} I_{th}^{\theta} \quad \ldots\ldots\ldots\ldots\ldots\ldots (9)$$

where "I_{th}^{θ}" is the bottom-hat transformed image, "S_e" is the structuring elements for morphological closing, "I" is the image to be processed, "$\bullet$" and "θ" is the angular rotation of the structuring element. If the closing along a class of linear structuring elements is considered, a sum of bottom-hat along each direction will brighten the vessels regardless of their direction, provided that the length of the structuring elements is larger enough to extract the vessel with the largest diameter. Inspired by Fraz's work [35], in our experiment, we set the structuring element to be 21 pixels long 1 pixel wide and the element is rotated at an angle spanning $[0, 8\pi/9]$ in step of $\pi/9$. **Fig. 5** shows the sum of bottom-hat "Is_{th}," which is the summation of the bottom-hat transformation. The set "A" in Eq. (9) consists of the angular orientations of structuring element and can be defined as $\{x | 0 \leq x \leq 8\pi/9 \,\&\, x \bmod (\pi/9) = 0\}$. As can be seen in **Fig. 5**, the sum of the bottom-hat on the retinal image will enhance all vessels, even some small or tortuous vessels. Besides, the bright zones can also be eliminated as shown in **Fig. 5(c)**.

3.4. ELM Classifier

Extreme learning machine (ELM) [38, 39] has been proposed for training single hidden layer feed-forward neural networks (SLFN). The method randomly chooses hidden nodes and analytically determines the output weights of SLFN. In theory, this algorithm tends to provide good generalization performance at extremely fast learning speed. **Fig. 6** shows the structure of ELM classifier, one can clearly see that the ELM includes input layer, hidden nodes and output layer. In the structure, the input and output nodes are respectively represented by the left and right squares and the hidden nodes are represented by the middle hexagons. In our experiment, the activation functions in the hidden nodes are set as the sigmoid function. The weights and biases parameters connect all the nodes. The core idea of ELM is randomly initializing the SLFN hidden nodes including internal weights and biases. In this way, the time-consuming training process can be largely improved.

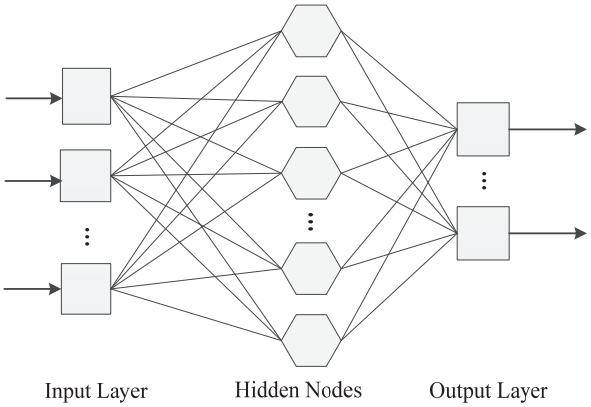

Fig. 6. The structure of ELM classifier.

For ELM, after the input weights and the hidden layer biases are chosen randomly, SLFN can be simply considered as a linear system and the output weights (linking the hidden layer to the output layer) of SLFN can be analytically determined through simple generalized inverse operation of the hidden layer output matrices. Therefore, ELM is remarkably efficient and tends to reach a global optimum.

Considering n samples $(\boldsymbol{x}_i, y_i), 1 \leq i \leq n$, with $\boldsymbol{x}_i \in \boldsymbol{R}^p$ and $y_i \in \boldsymbol{R}$, a SLFN with m hidden neurons in the hidden layer can be written as:

$$\hat{y}_i = \sum_{j=1}^{m} \beta_j f(w_j x_i + b_j), \quad 1 \leq i \leq n \quad \ldots\ldots (10)$$

where w_j and b_j are respectively represent the randomly initialized input weight and the bias. $f(\cdot)$ is an activation function and the sigmoid function is employed here. β_j is the j-th output weight. Denote the j-th output estimated by the SLFN as $\hat{y}_i$, in the hypothetical case where the SLFN perfectly approximates the actual output y_i, the relation

$$\sum_{j=1}^{m} \beta_j f(w_j x_i + b_j) = y_i, \quad 1 \leq i \leq n \quad \ldots\ldots (11)$$

can be written as $\boldsymbol{H}\beta = \boldsymbol{y}$, with

$$\boldsymbol{H} = \begin{pmatrix} f(w_1 x_1 + b_1) & \cdots & f(w_m x_1 + b_m) \\ \vdots & \ddots & \vdots \\ f(w_1 x_n + b_1) & \cdots & f(w_m x_n + b_m) \end{pmatrix} \quad . (12)$$

$\beta = (\beta_1, \beta_2, \ldots, \beta_m)^T$, and $\boldsymbol{y} = (y_1, y_2, \ldots y_m)^T$. Here, the parameters w_j and b_j are randomly initialized in ELM. In our experiments, let the size of the training feature matrix be $R \times Q$, the generated weight w_j is an $R \times Q$ random matrix and the bias b_j is also a random matrix, whose size

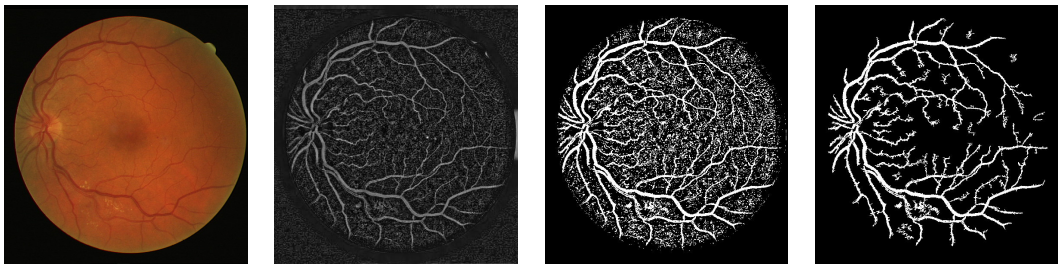

(a) (b) (c) (d)

Fig. 7. Image post-processing result. (a) Input retinal image. (b) Combined vessel image. (c) Merged binary vessel image. (d) Final vessel segmentation result.

is $N \times 1$. Thus, the output weights β can be calculated as:

$$\beta = \boldsymbol{H}^{\dagger} y \quad \ldots\ldots\ldots\ldots\ldots\ldots (13)$$

In Eq. (13), $\boldsymbol{H}^{\dagger}$ is the Moore-Penrose pseudo-inverse of $\boldsymbol{H}$. Once β and other random parameters are obtained, they can be used to classify the testing data using Eq. (10). The main steps for the ELM classifier are presented as follows:

ELM algorithm
Input: training data and the corresponding classes
Output: estimated ELM parameters: w_i, b, β
Step 1: The active function f is set as the sigmoid function, and the number of hidden nodes is set as m;
Step 2: The input weight w_i and bias b are randomly initialized;
Step 3: The hidden layer output matrix $\boldsymbol{H}$ is calculated by using Eq. (12);
Step 4: The output weight β is obtained by using Eq. (13).

Specifically, the ELM classifier used in the proposed vessel segmentation method includes the procedures of training and testing phases. In the training process, for each training image the input matrix of training set is defined as a 7-D feature vector, and the output matrix of training set is defined as the manual segmentation result represented by a binary matrix. The number of hidden neurons is set to 1000, and the sigmoid function is chosen as the transfer function of the ELM classifier. Thus, the input weight matrix w_i, bias matrix b and layer weight matrix β are obtained, which are used as the input parameters for the testing process. In the testing process, we use the ELM to classify the test data, and the classifier assigns one of the classes (vessel or non-vessel) to each candidate pixel when its representation in feature space is obtained. The output of the testing process is then converted to a vessel image.

3.5. Image Post-Processing

In our experiment, we find that the vessel image obtained by the ELM classifier seems lose some small vessel parts. Therefore, a combination of ELM classification result and bottom-hat transformation is used for the post-processing. Bottom-hat transformation is used to restore the connectivity of some small vessel parts by revealing some hidden pixels that belong to the blood vessel, as shown in **Fig. 7(b)**. Then, the combined image is merged with the binary mask image provided by the public DRIVE database to restrict pixels only inside the image field of view (FOV). This merging is accomplished through the classic AND operator. **Fig. 7(c)** shows the resultant binary image. As can be seen in **Fig. 7(c)**, the merged image contains some unwanted ledges and falsely-detected isolated vessel pixels. Therefore, 8-connected component analysis is used here. Every isolated part is labeled as a component. If the area of the component is less than 100 pixels, the component will be regarded as the falsely-detected isolated vessel parts to be removed from the binary image. **Fig. 7(d)** shows the final vessel segmentation result.

4. Experimental Evaluation

In this section, we first introduce the retinal image database and the assessment indexes that used in our experiments. Based on these materials, two criteria have been considered to verify the effectiveness and validity of the proposed method: (i) performance measures, and (ii) method evaluation. All the segmentation algorithms were performed by executing MATLAB on a PC with 3.00GHz Intel Pentium Dual-Core Processor.

4.1. Materials

The proposed algorithm is first applied for real captured retinal images. In our experiments, the TOPCON TRC-NW400 non-mydriatic fundus camera is used to collect fundus images. The images were collected from 36 subjects, and the subjects were chosen from among voluntary undergraduate and graduate students. The total number of collected test images is 82, and the size of each test image is 1956×1934.

To train the ELM classifier, some image samples were selected from the DRIVE database [24, 40] for our method, and the relevant parameters obtained by the train phase were used for segmenting the vessels from any real captured retinal images. **Fig. 8** shows some examples of vessel segmentation results for the images. As can be seen in the figure, using the proposed method the blood vessels in the real captured images can be segmented even in those uneven illumination areas, which demonstrate the effectiveness and robustness of our method.

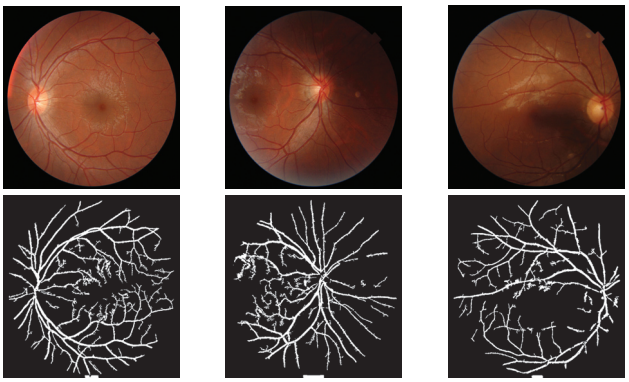

Fig. 8. Image segmentation results for real-captured retinal images. First row: real-captured images. Second row: corresponding vessel segmentation results.

Table 1. Vessel classification.

	Vessel present	Vessel absent
Vessel detected	True positive (TP)	False positive (FP)
Vessel not detected	False negative (FN)	True negative (TN)

Table 2. Performance indexes that used for blood vessel segmentation.

Measure	Description
SN	TP/(TP+FN)
SP	TN/(TN+FP)
Acc	(TP+TN)/(TP+FP+TN+FN)
PPV	TP/(TP+FP)

Then, the proposed algorithm was tested on DRIVE database images to compare with existing works. 40 TIFF formatted RGB retinal images with a size of 565 × 584 pixels are included in the DRIVE database, and the database images are divided into 20 training images and 20 testing images. Manually labeled retina images created by two human observers (pathologists) are also contained in the testing database. These manually labeled images are used for comparison with the images acquired from training set. Although both of the manually labeled images can be used in comparisons, only the first observer's performance is regard as Gold Standard just like many researchers' work.

As illustrated in **Table 1**, in binary classification, the true positive refers to any pixel which is identified as vessel by the algorithm and is also marked as vessel in the ground truth, while the false positive refers to any pixel which is marked as vessel in the segmented image but not in the ground truth image.

The measurements used for evaluating algorithm performance are: Accuracy (Acc), Sensitivity (SN), Specificity (SP), and Positive Predictive Value (PPV) [35]. **Table 2** shows the definition of these performance indexes that used for vessel segmentation. As can be seen in the table, Sensitivity (SN) reflects the ability of an algorithm to detect the vessel pixels. Specificity (SP) is the ability to detect non-vessel pixels. The accuracy (Acc) is measured by the ratio of the total number of correctly classified pixels (sum of true positives and true negatives) by the number of pixels in the image FOV. The Positive Predictive Value (PPV) or precession rate gives the proportion of identified vessel pixels which are true vessel pixels.

Table 3. Performance indexes for the images in the DRIVE database.

Index	TP	FP	FN	TN
2nd Human Observer	22349.10	5412.10	6548.15	295649.15
Proposed Method	**22358.75**	**5142.15**	**6569.55**	**291120.60**
Index	**SN**	**SP**	**Acc**	**PPV**
2nd Human Observer	0.7734	0.9820	0.9638	0.8050
Proposed Method	**0.7729**	**0.9826**	**0.9640**	**0.8130**

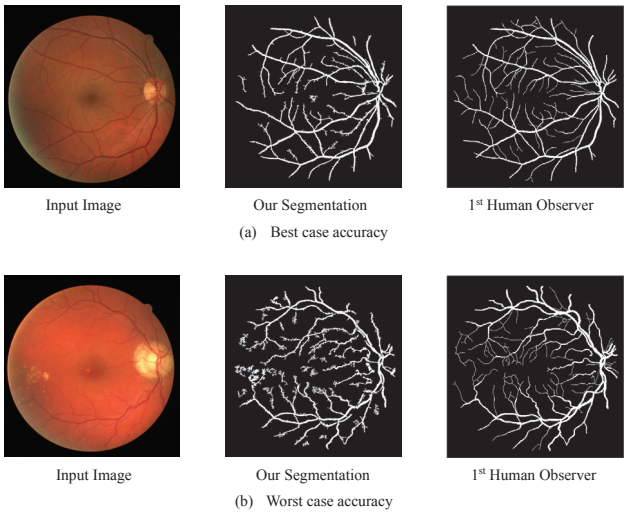

Fig. 9. Image segmentation results for the images in DRIVE database.

4.2. Performance Measures

In our experiments, we apply the proposed algorithm on 20 DRIVE test images. By taking the first human observer as the ground truth, the performance of the proposed algorithm can be effectively measured. **Table 3** shows the average of the selected indexes of algorithm performance for the DRIVE database.

As can be seen in **Table 3**, compared with the second human observers for the DRIVE database, the average accuracy values and precision rates obtained by the proposed algorithm are larger. Besides, the proposed algorithm also has higher value than the second human observer in terms of specificity for the image database, which indicates the low FP rate of the proposed method as compared with the second human observer. Therefore, we can deduce that the proposed algorithm has identified less numbers of wrong pixels (e.g. background pixels or pathological area pixels) as part of a vessel than the second human observer. **Fig. 9** shows the image segmentation results with the best case and worst case accu-

Table 4. Performance measurement for vessel segmentation methods (DRIVE images).

No	Type	Methods	Year	SN	SP	Acc
1.	Unsupervised Method	2nd Human Observer	-	0.7796	0.9717	0.9470
8.		Fraz [11]	2011	0.7152	0.9759	0.9430
9.		You [28]	2011	0.7410	0.9751	0.9434
10.		Oliveira [7]	2012	N.A	N.A	0.9566
11.		Dai [14]	2013	0.6542	0.9759	0.9347
12.		Masooomi [15]	2014	0.7345	0.9629	0.9425
13.		Wankhede [21]	2015	0.7261	0.9806	0.9626
14.		Singh [8]	2016	N.A	N.A	0.9522
15.	Supervised Method	Marin [27]	2011	0.7067	0.9801	0.9452
21.		Nandy [29]	2012	N.A	N.A	0.9616
22.		Ceylan [30]	2013	N.A	N.A	0.9856
23.		Ding [31]	2014	N.A	N.A	0.9120
24.		Melinscak [32]	2015	N.A	N.A	0.9466
25.		Li [33]	2016	0.7569	0.9816	0.9527
26.		**Proposed Method**	**2016**	**0.7729**	**0.9826**	**0.9640**

N.A = Not Available

racy from the DRIVE database. For the DRIVE database, the best case Acc, SN, SP, and PPV are 0.9684, 0.8335, 0.9856, and 0.7950, respectively, and the worst case measures are 0.9369, 0.7408, 0.9553, and 0.6096, respectively.

4.3. Method Evaluation

We compare the performance of the proposed method with that of existing algorithms shown in **Table 4** for the DRIVE database. The SN, SP and Acc of the proposed algorithm are compared with the results of existing methods. In **Table 4**, the performance measure of existing segmentation methods are directly from the websites or their published papers.

Figure 10 shows the comparison between the existing representative algorithms (e.g., some algorithms [14, 32] enumerated in **Table 4**) and the proposed method. One can clearly see that although the previous algorithms can obtain a relatively good vessel segmentation results for the input retinal images shown in **Fig. 10**, Dai's method [14] yields a lower sensitivity that is mainly because of the width of vessel is not accurate and an high threshold value applied to reduce the noises introduce by the phase congruency. While Melinscak's method [32] requires a relatively long time to construct deep max-pooling convolutional neural networks for segmenting blood vessels. In contrast, our proposed method can keep a balance between the accuracy and the speed.

The accuracy (Acc) is one of the most important criteria in measuring the performance of vessel segmentation algorithms. The comparative analysis shows that the

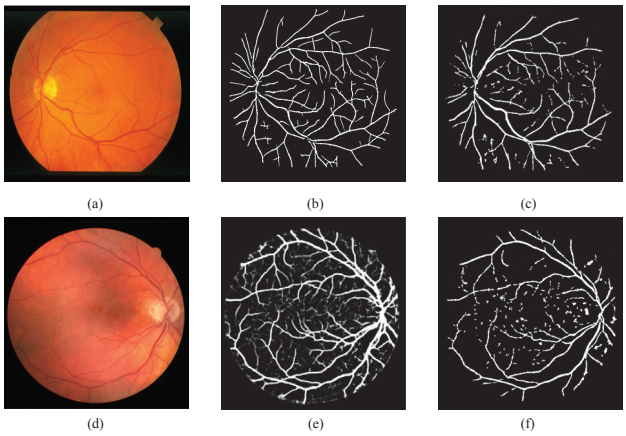

Fig. 10. Comparison with Dai's work and Melinscak's work. (a) and (d) are input retinal images. (b) is Dai's vessel segmentation result. (e) is Melinscak's vessel segmentation result. (c) and (f) are our vessel segmentation results.

proposed algorithm can achieve a relatively good performance. As can be seen in **Table 4**, our method renders better Acc than most other algorithms for the DRIVE database. The method outperforms our method in terms of Acc only by Ceylan et al. [30] (0.9856). Ceylan's technique used 4th level Complex Wavelet Transform and Complex-Valued ANN for the blood vessels segmentation, which is proved to be very effective to segment blood vessel in retinal image. However, the method share the common limitation of most ANN based methods – the training phase costs too much time. The ELM that used in our method is different compared to the ANN based method. Since the hidden node parameters of ELM are completely independent from the training data, it can thus tend to afford generalization performance at very fast learning speed. Besides, apart from the fast computational speed, the strength of the proposed method also lies in its capturing a rich collection of shape, structural information, and local information at multiple spatial scales in the feature vector.

To be more specific, one of the main advantages of the proposed method is its simplicity. The method only computes seven features for pixel classification, and the ELM based classifier used in training phase can be analytically determined rather than being tuned. Thus, compared with other classifier, the proposed method utilizes less computational times. For example, the Gaussian Mixture Model (GMM) classifier used in Soares's method [25] is trained in approximately 8 hours. The total time required to process a single image is about 100 seconds, running on a PC with an Intel Core2Duo CPU at 2.27GHz and 4GB of RAM. For Li's method [33], the average time required to train the deep neural network for one dataset is about 7 hours with an AMD Athlon II X4 645 CPU running at 3.10 GHz with 4 GB of RAM. In comparison, our method only needs 55 seconds in the training phase to obtain the relevant parameters and experimental results also show that it can maintain a good trade-off between accuracy and training time. Since the method is experimentally

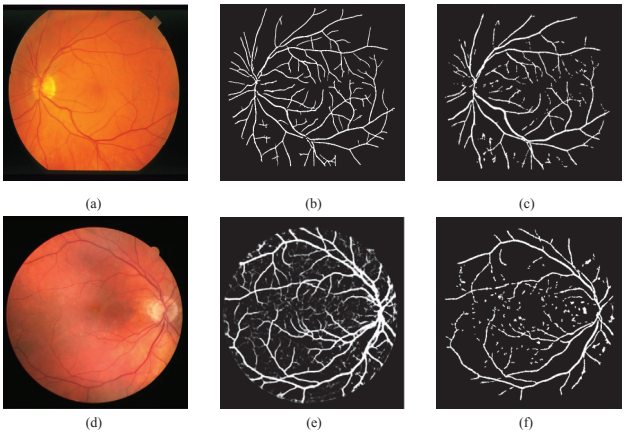

Fig. 11. Comparison of segmentation results on retinal images with pathological condition and uneven illumination. From left to right: input image, vessel segmentation images obtained by the proposed method and vessel segmentation images obtained by Soares's method.

implemented in MATLAB, this performance can still be improved.

Besides, blood vessel segmentation also faces many challenges, such as lesions in the retinal vasculature, uneven illumination, etc. **Fig. 11** shows the comparison results of the segmented images in pathological and non-uniform illumination conditions. The result images that used for comparing with our method's results are directly downloaded from Soares' website [41]. One can clearly see that the proposed method performs better in removal of pathological artifacts and uneven illumination areas.

5. Discussion

In this section, we mainly discuss some critical issues, such as technique challenges, limitations, and possible solutions that relate to the technique contribution of the proposed method.

Retinal blood vessel segmentation faces many technique challenges: a) the presence of lesions and noise; b) uneven illumination; c) drift in intensity; d) lack of image contrast between background and vessel regions; e) varying vessel width; f) central vessel reflex.

Although some measures have been taken to solve a part of the above problems using unsupervised or supervised schemes, the proposed algorithm as a supervised method shows comparative performance against other methods. However, the proposed method also has some limitations: a) the vessel segments in our resulted binary images are thicker than vessels in gold standard images. Therefore, the segmentation performances will be decreased; b) supervised methods are notoriously expensive during training, and the proposed method is no exception. Our MATLAB prototype was tested on a PC with a 3.10 GHz Intel Pentium Dual-Core Processor. In our experiments, generating the 7-D feature vector in the training phase took about 55 seconds, and classifying a retinal image with a size of 565×584 pixels costs about 8 seconds. Considering that the proposed algorithm will be incorporated into assisted-diagnosis systems and expected to supply an answer within a limited time, thus although the computing speed of the proposed method is faster than most existing supervised vessel segmentation methods, its computation time should be further reduced; c) green channel, multi-scale Gabor filter, Hessian matrix and bottom-hat transformation are chosen as our extracted features for retinal images. However, which feature is most important in the vessel and non-vessel classification task is not studied in our work. Nevertheless, we provide a new way to solve the problem of automatic retinal blood vessel segmentation, which is quite essential for retinal image analysis system.

In the future, we intend to investigate the following possible solutions to enhance the flexibility of the proposed algorithm: a) incorporating the vessel width and tortuosity measures into the proposed algorithm; b) developing an interactive vessel analysis software tool for ophthalmologists; c) minimizing the computation times to meet the needs of practical requirements; d) choosing more proper feature vector and training data to improve the efficiency and accuracy of the retinal vessel segmentation; e) testing our algorithm on further and larger database of annotated vessels and cooperating with clinical partners.

6. Conclusions

In this paper, we have proposed a very simple but effective supervised method for automated segmentation of blood vessels in retinal images using an ELM classifier. We have used a 7-D vector to represent retinal image features. The feature vector consists of green channel, multi-scale Gabor filter, Hessian matrix and bottom-hat transformation. These feature vectors can deal with both normal and pathological retinas. To verify the effectiveness of the proposed algorithm, we test the proposed method on the real-captured images and public DRIVE database images. The demonstrated performance, effectiveness and robustness along with its simplicity in training as well as in classification, make the ELM based method for blood vessel segmentation a suitable tool to be integrated into a retinal image analysis system for clinical purposes. Therefore, many applications in medical field can benefit from the proposed method.

Acknowledgements

This work was supported in part by the National Natural Science Foundation of China (No.61502537, 61573380, 61702559), Postdoctoral Science Foundation of Central South University (No.126648).

References:

[1] C. A. Lupascu, D. Tegolo, and E. Trucco, "FABC: Retinal vessel segmentation using adaboost," IEEE Trans. on Information Technology in Biomedicine. Vol.14, No.5, pp. 1267-1274, 2010.

[2] Y. Koga, A. Yamamoto, H. Kim, J. K. Tan, and S. Ishikawa, "Detection of artery regions in lower extremity arteries from non-enhanced MR imaging based on particle filter algorithms," J. Adv. Comput. Intell. Intell. Inform. (JACIII), Vol.17, No.2, pp. 318-323, 2013.

[3] M. M. Fraz, P. Remagnino, A. Hoppe, B. Uyyanonvara, A. R. Rudnicka, C. G. Owen, and S. A. Barman, "Blood vessel segmentation methodologies in retinal images – A survey," Computer Methods & Programs in Biomedicine, Vol.108, No.1, pp. 407-433, 2012.

[4] F. Jusoh, H. Haron, R. Ibrahim, and M. Z. C. Azemin, "An overview of retinal blood vessel segmentation," Advanced Computer and Communication Engineering Technology, Vol.362, pp. 63-71, 2015.

[5] A. D. Hoover, V. Kouznetsova, and M. Goldbaum, "Locating blood vessels in retinal images by piecewise threshold probing of a matched filter response," IEEE Trans. on Medical Imaging, Vol.49, No.2, pp. 168-172, 2000.

[6] L. Gamg, O. Chutatape, and S. M. Krishnan, "Detection and measurement of retinal vessels in fundus images using amplitude modified second-order Gaussian filter," IEEE Trans. on Biomedical Engineering, Vol.49, No.2, pp. 168-172, 2002.

[7] W. S. Oliveira, T. I. Ren, and G. D. C. Cavalcanti, "An unsupervised segmentation method for retinal vessel using combined filters," Proc. of IEEE 24th Int. Conf. on Tools with Artificial Intelligence, pp. 750-756, 2012.

[8] N. P. Singh and R. Srivastava, "Retinal blood vessels segmentation by using Gumbel probability distribution function based matched filter," Computer Methods and Programs in Biomedicine, Vol.129, pp. 40-50, 2016.

[9] F. Zana and J. C. Klein, "Segmentation of vessel-like patterns using mathematical morphology and curvature evaluation," IEEE Trans. on Image Processing, Vol.10, No.7, pp. 1010-1019, 2001.

[10] A. M. Mendonca and A. Campilho, "Segmentation of retinal blood vessels by combining the direction of centerlines and morphological reconstruction," IEEE Trans. on Medical Imaging, Vol.25, No.9, pp. 1200-1213, 2006.

[11] M. M. Fraz, S. A. Barman, P. Remagnino, A. Hoppe, A. basit, B. Uyyanonvara, A. R. Rudnickc, and C. G. Owen, "An approach to localize the retinal blood vessels using bit planes and centerline detection," Computer Methods & Programs in Biomedicine, Vol.108, No.2, pp. 600-616, 2012.

[12] F. K. H. Quek and C. Kirbas, "Vessel extraction in medical images by wave-propagation and traceback," IEEE Trans. on Medical Imaging, Vol.20, No.2, pp. 117-131, 2001.

[13] A. F. Frangi, W. J. Niessen, K. L. Vincken, and M. A. Viergever, "Multiscale vessel enhancement filtering," Medical Image Computing and Computer-Assisted Intervention, pp. 130-137, 1496.

[14] B. S. Dai, W. Bu, X. Q. Wu, and Y. L. Zheng, "Retinal blood vessel detection using multiscale line filter and phase congruency," Proc. of Int. Conf. on Image Processing, Computer Vision, & Pattern Recognition, pp. 1-7, 2013.

[15] R. Masooomi, A. Ahmadifard, and A. Mohtadizadeh, "Retinal vessel segmentation using non-subsampled contourlet transform and multi-scale line detection," Proc. of Iranian Conf. on Intelligent Systems, pp. 1-5, 2014.

[16] W. Li, A. Bhalerao, and R. Wilson, "Analysis of retinal vasculature using a multiresolution hermite model," IEEE Trans. on Medical Imaging, Vol.26, No.2, pp. 137-152, 2007.

[17] B. S. Y. Lam and Y. Hong, "A novel vessel segmentation algorithm for pathological retina images based on the divergence of vector fields," IEEE Trans. on Medical Imaging, Vol.27, No.2, pp. 237-246, 2008.

[18] B. S. Y. Lam, G. Yongsheng, and A. W. C. Liew, "General retinal vessel segmentation using regularization-based multiconcavity modeling," IEEE Trans. on Medical Imaging, Vol.29, No.7, pp. 1369-1381, 2010.

[19] H. Narasimha-Iyer, J. M. Beach, B. Khoobehi, and B. Roysam, "Automatic identification of retinal arteries and veins from dual-wavelength images using structural and functional features," IEEE Trans. on Biomedical Engineering, Vol.54, No.8, pp. 1427-1435, 2007.

[20] B. Al-Diri, A. Hunter, and D. Steel, "An active contour model for segmenting and measuring retinal vessels," IEEE Trans. on Medical Imaging, Vol.28, No.9, pp. 1488-1497, 2009.

[21] P. R. Wankhede and K. B. Khanchandani, "Retinal blood vessel segmentation using graph cut analysis," Proc. of Int. Conf. on Industrial Instrumentation and Control, pp. 1429-1432, 2015.

[22] K. W. Sum and P. Y.. S. Cheung, "Vessel extraction under non-uniform illumination: A level set approach," IEEE Trans. on Biomedical Engineering, Vol.55, No.1, pp. 358-360, 2008.

[23] M. Niemeijer, J. Staal, B. van Ginneken, M. Loog, and M. D. Abramoff, "Comparative study of retinal vessel segmentation methods on a new publicly available database," Proc. of SPIE, Vol.5370, pp. 648-665, 2004.

[24] J. Staal, M. D. Abramoff, M. Niemeijer, M. A. Viergever, and B. van Ginneken, "Ridge-based vessel segmentation in color images of the retina," IEEE Trans. on Medical Imaging, Vol.23, No.4, pp. 501-509, 2004.

[25] J. V. B. Soares, J. J. G. Leandro, R. M. Cesar, H. F. Jelinek, and M. J. Cree, "Retinal vessel segmentation using the 2-D Gabor wavelet and supervised classification," IEEE Trans. on Medical Imaging, Vol.25, No.9, pp. 1214-1222, 2006.

[26] E. Ricci and R. Perfetti, "Retinal blood vessel segmentation using line operators and support vector classification," IEEE Trans. on Medical Imaging, Vol.26, No.10, pp. 1357-1365, 2007.

[27] D. Marin, A. Aquino, M. E. Gegundez-Arias, and J. M. Bravo, "A new supervised method for blood vessel segmentation in retinal images by using gray-level and moment invariants-based features," IEEE Trans. on Medical Imaging, Vol.30, No.1, pp. 146-158, 2011.

[28] X. You, Q. Peng, Y. Yuan, Y. Cheung, and J. Lei, "Segmentation of retinal blood vessels using the radial projection and semi-supervised approach," Pattern Recognition, Vol.44, pp. 2314-2324, 2011.

[29] M. Nandy and M. Banerjee, "Retinal vessel segmentation using Gabor filter and artificial neural network," Proc. of 3rd Int. Conf. on Emerging Applications of Information Technology, pp. 157-160, 2012.

[30] M. Ceylan and H. Yasar, "Blood vessel extraction from retinal images using complex wavelet transform and complex-valued artificial neural network," Proc. of 36th Int. Conf. on Telecommunications and Signal Processing, pp. 822-825, 2013.

[31] C. Ding, Y. Xia, and Y. Li, "Supervised segmentation of vasculature in retinal images using neural networks," Proc. of IEEE Int. Conf. on Orange Technologies, pp. 49-52, 2014.

[32] M. Melinscak, P. Prentasic, and S. Loncaric, "Retinal vessel segmentation using deep neural networks," Proc. of 10th Int. Conf. on Computer Vision Theory and Applications, pp. 577-582, 2015.

[33] Q. L. Li, B. W. Feng, L. P. Xie, P. Liang, H. S. Zhang, and T. F. Wang, "A Cross-Modality Learning Approach for Vessel Segmentation in Retinal Images," IEEE Trans. on Medical Imaging, Vol.35, No.1, pp. 109-118, 2016.

[34] K. M. He, J. Sun, and X. O. Tang, "Guided image filtering," IEEE Trans. on Pattern Analysis and Machine Intelligence, Vol.35, No.6, pp. 1397-1409, 2013.

[35] M. M. Fraz, P. Remagnino, A. Hoppe, B. Uyyanonvara, A. R. Rudnicka, C. G. Owen, and S. A. Barman, "An ensemble classification-based approach applied to retinal blood vessel segmentation," IEEE Trans. on Biomedical Engineering, Vol.59, No.9, pp. 2538-2548, 2012.

[36] A. Frangi, W. J. Niessen, K. Vincken, and M. Viergever, "Multiscale vessel enhancement filtering," Medical Image Computing and Computer-Assisted Intervention, Vol.1496, pp. 130-137, 2006.

[37] E. Aswini, S. Divya, S. Kardheepan, and T. Manikandan, "Mathematical morphology and bottom-hat filtering approach for crack detection on relay surfaces," Proc. of IEEE Int. Conf. on Smart Structures and Systems, pp. 108 -113, 2013.

[38] G. B. Huang, Q. Y. Zhu, K. Z. Mao, C. K. Siew, P. Saratchandran, and N. Sundararajan, "Can threshold networks be trained directly?," IEEE Trans. on Circuits & Systems II Express Briefs, Vol.53, No.3, pp. 187-191, 2006.

[39] G. B. Huang, H. Zhou, X. Ding, and R. Zhang, "Extreme learning machine for regression and multiclass classification," IEEE Trans. on Systems Man & Cybernetics Part B Cybernetics, Vol.42, No.42, pp. 513-529, 2012.

[40] http://www.isi.uu.nl/Research/Databases/DRIVE [accessed May 15, 2015]

[41] http://www.ces.clemson.edu/_ahoover/stare/probing/index.html/ [accessed May 1, 2015]

Name:
Fan Guo

Affiliation:
Lecturer, School of Information Science and Engineering, Central South University

Address:
Changsha, Hunan 410083, China

Brief Biographical History:
2005 Received B.S. Degree from Central South University
2008 Received M.S. Degree from Central South University
2012 Received Ph.D. Degree from Central South University

Main Works:
• "Automatic Retinal Image Registration Using Blood Vessel Segmentation and SIFT Feature," Int. J. of Pattern Recognition and Artificial Intelligence, Vol.31, No.11, pp. 1-25, 2017.
• "Adaptive Estimation of Depth Map for Two-Dimensional to Three-Dimensional Stereoscopic Conversion," Optical Review, Vol.21, No.1, pp. 60-73, 2014.

Membership in Academic Societies:
• The Institute of Electrical and Electronics Engineers (IEEE)
• China Computer Federation (CCF)
• Chinese Association for Artificial Intelligence (CAAI)

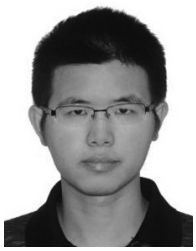

Name:
Da Xiang

Affiliation:
Master Student, School of Information Science and Engineering, Central South University

Address:
Changsha, Hunan 410083, China

Brief Biographical History:
2016 Received B.S. Degree from Central South University
Currently pursuing a M.S. Degree in control engineering from Central South University

Name:
Beiji Zou

Affiliation:
Professor, School of Information Science and Engineering, Central South University

Address:
Changsha, Hunan 410083, China

Brief Biographical History:
1978-1982 B.S. Degree from Zhejiang University
1982-1984 M.S. Degree from Tsinghua University
1997-2001 Ph.D. Degree from Hunan University
2001-2003 Postdoctoral Researcher, Tsinghua University

Main Works:
• "Hierarchical contour closure-based holistic salient object detection," IEEE Trans. on Image Processing, Vol.26, No.9, pp. 4537-4552, 2017.
• "Motion recognition for 3D human motion capture data using support vector machines with rejection determination," Multimedia Tools and Applications, Vol.70, No.2, pp. 1333-13625, 2014.
• "A novel particle filter with implicit dynamic model for irregular motion tracking," Mach. Vis. Appl., Vol.24, No.7, pp. 1487-1499, 2013.

Membership in Academic Societies:
• The Institute of Electrical and Electronics Engineers (IEEE)
• China Computer Federation (CCF)

Name:
Chengzhang Zhu

Affiliation:
Lecturer, College of Literature and Journalism, Central South University

Address:
Changsha, Hunan 410083, China

Brief Biographical History:
2016 Received Ph.D. degree from Central South University

Main Works:
• "Retinal vessel segmentation in colour fundus images using Extreme Learning Machine," Computerized Medical Imaging and Graphics, Vol.55, pp. 68-77, 2017.
• "An Ensemble Retinal Vessel Segmentation Based on Supervised Learning in Fundus Images," Chinese J. of Electronics, Vol.25, No.3, pp. 503-511, 2016.

Membership in Academic Societies:
• China Computer Federation (CCF)

Name:
Shengnan Wang

Affiliation:
Undergraduate Student, School of Information Science and Engineering, Central South University

Address:
Changsha, Hunan 410083, China

Brief Biographical History:
Currently pursuing a B.S. degree in computer science and technology from Central South University